Scattering properties of ultrafast laser-induced refractive index shaping lenticular structures in hydrogels

Kaitlin T. Wozniak[a], Thomas A. Germer[b], Sam C. Butler[c,e], Daniel R. Brooks[a], Krystel R. Huxlin[d], Jonathan D. Ellis[a,c,f]

[a]The Institute of Optics, University of Rochester, 275 Hutchison Rd., Rochester, NY 14620; [b]National Institute of Standards and Technology, 100 Bureau Dr., Gaithersburg, MD 20899; [c]Department of Mechanical Engineering, University of Rochester, 233 Hopeman Engineering Building, Rochester, NY 14627; [d]Flaum Eye Institute, University of Rochester, 210 Crittenden Blvd. Box 314, Rochester, NY 14642; [e]Clerio Vision, Inc, 1255 University Ave., Suite 210, Rochester, NY 14607; [f]College of Optics Sciences, University of Arizona, 1630 E University Blvd, Tucson, AZ 85719

ABSTRACT

We present measurements of light scatter induced by a new ultrafast laser technique being developed for laser refractive correction in transparent ophthalmic materials such as cornea, contact lenses, and/or intraocular lenses. In this new technique, called intra-tissue refractive index shaping (IRIS), a 405 nm femtosecond laser is focused and scanned below the corneal surface, inducing a spatially-varying refractive index change that corrects vision errors. In contrast with traditional laser correction techniques, such as laser *in-situ* keratomileusis (LASIK) or photorefractive keratectomy (PRK), IRIS does not operate via photoablation, but rather changes the refractive index of transparent materials such as cornea and hydrogels. A concern with any laser eye correction technique is additional scatter induced by the process, which can adversely affect vision, especially at night. The goal of this investigation is to identify sources of scatter induced by IRIS and to mitigate possible effects on visual performance in ophthalmic applications. Preliminary light scattering measurements on patterns written into hydrogel showed four sources of scatter, differentiated by distinct behaviors: (1) scattering from scanned lines; (2) scattering from stitching errors, resulting from adjacent scanning fields not being aligned to one another; (3) diffraction from Fresnel zone discontinuities; and (4) long-period variations in the scans that created distinct diffraction peaks, likely due to inconsistent line spacing in the writing instrument. By knowing the nature of these different scattering errors, it will now be possible to modify and optimize the design of IRIS structures to mitigate potential deficits in visual performance in human clinical trials.

Keywords: diffraction, femtosecond, ophthalmic hydrogel, photo-modification, scatter, vision correction

1. INTRODUCTION

Since the invention of ultrashort, pulsed lasers in the 1970s, ultrafast lasers have found a variety of applications, including biomedical, industrial, and scientific. Laser-based photo-modification has gained significant interest from its ability to create 3D structures in transparent materials[1]. Tightly focusing femtosecond laser pulses in a transparent medium creates a high peak intensity in the focal region, allowing for highly localized material changes via multi-photon absorption in the bulk material. These changes include structural or chemical changes, as well as optical breakdown of the material. Femtosecond photo-modification uses multi-photon absorption to either remove material via photoablation, creating surface structures or to modify material properties, such as refractive index (RI).

In transparent bulk materials, studies have found RI change values as large as 1×10^{-2} in glass and 1×10^{-3} in polymeric materials like polymethyl methacrylate (PMMA).[2-4] The laser parameters for femtosecond photo-modification can vary widely depending on the intended use. At low repetition rates (10 Hz to 1 MHz), each pulse creates a material modification localized to the focal region.[5] At high repetition rates (greater than 1 MHz), heat accumulation also becomes a significant factor in the laser material interaction.[6] In this case, the thermal diffusion time is longer than the time between pulses, and while the laser-material interaction is still restricted to the focal volume, the cumulative effect of the laser pulses creates a more symmetric, spatially-uniform modification profile.[7] Since pulse energy is inversely proportional to repetition rate, high repetition rate lasers have lower pulse energies (nanojoules) than low repetition rate lasers. Multi-photon absorption is peak-power dependent; therefore, at low pulse energies, only the central part of the laser focal volume has sufficient energy to exceed the nonlinear absorption threshold and modifications are limited to that region. By combining the effects

of high repetition rate and low pulse energies, femtosecond lasers can create uniform 3D structures, with sizes on the order of the focal spot, in bulk transparent materials.[6,8]

In 2006, Ding *et al.* demonstrated the ability to create large refractive index changes in silicone- and non-silicone-based hydrogel polymers using a tightly focused femtosecond laser.[9] A mode-locked Ti:Sapphire femtosecond laser, operating at 800 nm, with a repetition rate of 93 MHz and pulse energies of 1.3 nJ, induced refractive index change, Δn, in hydrogels as large as 0.06. Recent advances have produced bulk phase change exceeding one wave (535 nm).[10] This technique has since been expanded for use in ophthalmic applications. Namely, large area refractive patterns have been created in ophthalmic hydrogels normally used for contact lenses and intraocular lenses.[10,11] Successful implementation of femtosecond photo-modification to such materials could provide a means for high-throughput, custom refractive corrections in ophthalmic hydrogels.[12]

In 2008, it was shown that femtosecond photo-modification could also be performed in cornea.[13] Unlike traditional refractive surgeries, such as LASIK and PRK, which correct vision errors by reshaping the anterior corneal surface via photoablation, IRIS was able to locally change the refractive index of the cornea to create 3D refractive structures.[13-18]. The high repetition rate, low pulse energy femtosecond laser employed in IRIS operates below the damage threshold of cornea, offering a non-surgical alternative to traditional laser vision correction methods.[19] To date, the main use of IRIS has been to inscribe gradient index (GRIN) layers in the mid-stromal region of the cornea. By controlling the amount of RI change induced, phase-wrapped Fresnel lenses as well as cylindrical GRIN lenses have been inscribed in both *ex vivo* and *in vivo* feline corneas, as well as in *ex vivo* human corneas.[14,16,19-21]

However, for IRIS to be implemented as a vision correction technique in cornea, or as a scalable manufacturing process for ophthalmic hydrogels, the optical performance of IRIS refractive structures must be assessed and controlled. Here, we measured scatter magnitudes arising from IRIS performed in hydrogel tissue surrogates. We identified four different sources of scatter in our samples. This information is critical for optimizing IRIS designs for ophthalmic applications, since scatter can adversely affect visual acuity.[22-25]

2. METHODOLOGY

2.1 IRIS instrumentation and procedure

IRIS creates bulk phase change in transparent ophthalmic materials by scanning the focal spot of a 405 nm, femtosecond laser through the material. We used a mode-locked Ti:Sapphire laser, which output 810 nm, 100 fs pulses at a repetition rate of 80 MHz. The light was frequency doubled by second harmonic generation. After passing through a 2D orthogonal mirror galvanometer, the beam was relayed through a unit magnification Keplerian telescope to the entrance pupil of a microscope objective (Fig. 1). A two-axis galvanometer system, in combination with three linear stages, controlled the position of the focal volume within the sample. The beam was moved in a raster scan pattern to create 3D refractive structures.

The IRIS process depends on many parameters, including peak laser power within the focal volume, line spacing for the raster scan pattern, scan speed of the focal spot within the material, laser spot parameters (waist and Rayleigh length), and material response. The peak power in the focal region is dependent on the average power, pulse width, and repetition rate. For intensity control, the laser was focused into an acousto-optic modulator (AOM) with megahertz bandwidth.[26] The AOM was synchronized to the galvanometer scanning to enable control of RI change along scan lines. While the nominal pulse width of the laser was 100 fs, positive dispersion from optical elements in the system can stretch that pulse to approximately 400 fs. To compensate for this dispersion and minimize the pulse width, the laser was bounced between two Gires-Tournois interferometer (GTI) mirrors. This study used the nominal 80 MHz laser repetition rate for all experiments. The orthogonal galvanometer mirror system was used to create a raster pattern with 0.5 μm line spacing. The line width of the written region was approximately 1.3 μm, thus the 0.5 μm line spacing was chosen to create a high fill factor, resulting in a continuous RI change within the sample. The line spacing is determined by the motion of the linear stages and is an adjustable parameter. The motion of the focal spot was primarily controlled by the galvanometer, and a scan speed of 200 mm/s was used for these experiments.

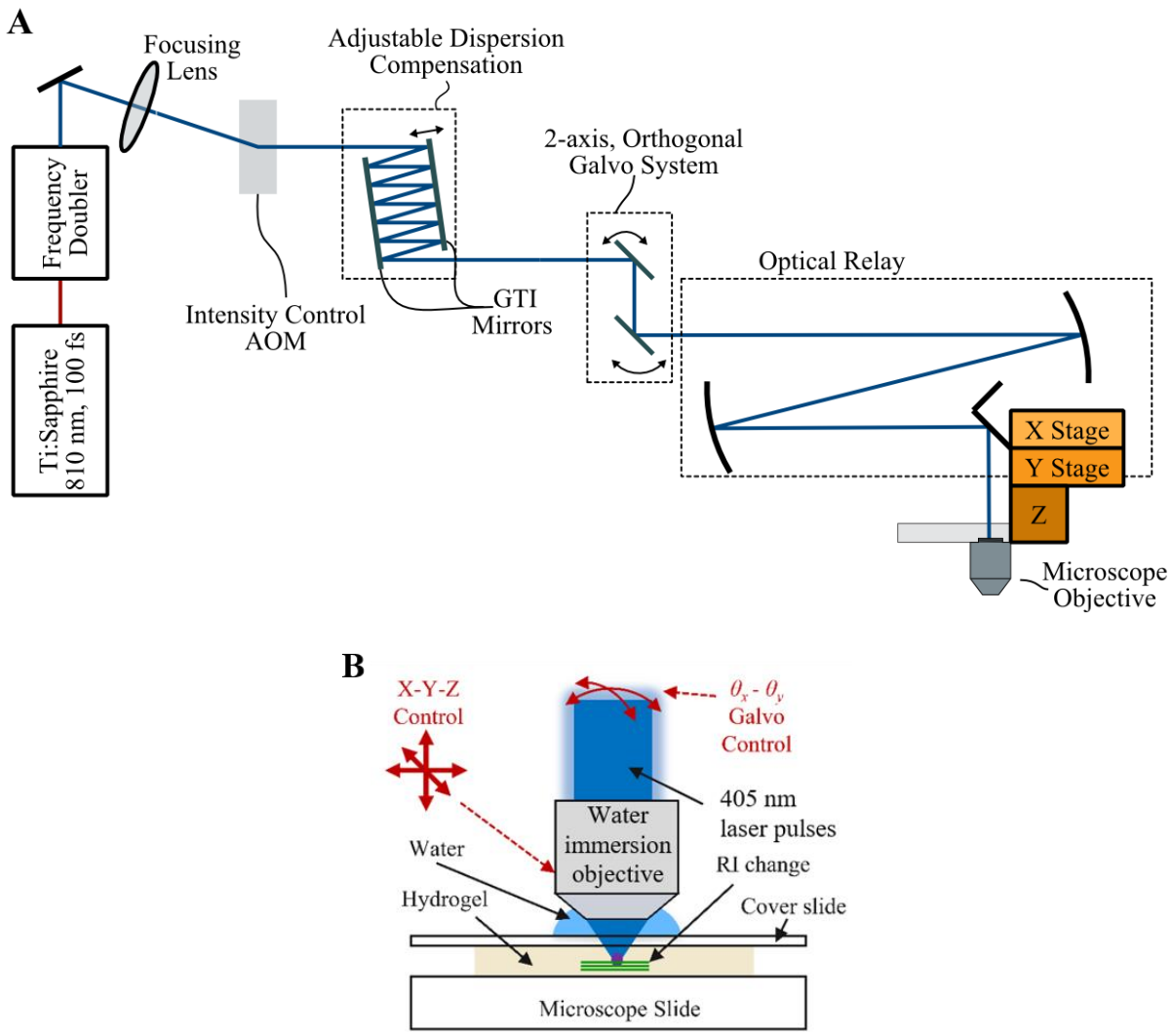

Figure 1. **IRIS schematic. A**. Diagram showing the main elements of the setup used for IRIS. After frequency doubling to 405 nm, the femtosecond pulses passed through an AOM at the Bragg angle. The intensity of the laser was controlled by modulating the first order diffraction efficiency. To compensate for dispersion of the optical elements in the setup, the beam bounced between two GTI mirrors. A two axis, orthogonal galvanometer system, in conjunction with linear stages, was used to raster scan the focal region within a sample to create 3D refractive structures. **B.** Diagram illustrating how refractive structures were written into hydrogel materials.

As noted earlier, IRIS can be used to create arbitrary refractive structures in both ophthalmic hydrogels and corneal tissue; the instrumentation and procedure for both materials is identical except for the effective numerical aperture (NA) used to focus the femtosecond pulses. In cornea, the native two-photon absorption of the stroma drives the IRIS process. The water immersion objective chosen for IRIS can achieve a NA of 1.0. However, higher NA leads to tissue damage at lower powers, without a significant increase in bulk phase change. Therefore, an effective NA between 0.5 and 0.7 is employed for corneal IRIS procedures by reducing the beam size at the entrance pupil of the objective.[16,17,27] For hydrogels, previous experiments used an effective NA of approximately 0.6.[10] Recent studies have found that reducing the effective NA led to higher bulk phase changes in hydrogel materials. For this study, an effective NA of 0.19 was used for the majority of the hydrogel samples. However, some samples were also written using a higher NA (0.49) for a comparative assessment of optical quality.

2.2 IRIS refractive structures

Traditional laser refractive surgeries correct optical aberrations of the eye by reshaping the anterior corneal surface, thus modifying the optical power of the eye. In IRIS, the refractive correction occurred by inscribing GRIN lenses in the mid-stromal region of the cornea, changing its optical power by modifying its RI. In order to create arbitrary refractive structures, calibration functions for IRIS-induced RI change as a function of exposure parameters were necessary. Small areas of constant phase were written in hydrogel materials with varied exposure parameters, then measured using a Mach-Zehnder interferometer. Once calibration functions were characterized, it was possible to create GRIN refractive structures by controlling the exposure parameters (as described in the previous section) at discrete intervals in the material as the laser scanned the sample to locally control the induced amount of RI change. To create refractive devices, a numerical value for RI change must be known for all sets of exposure parameters. However, for visual applications, the quantity of interest is the change in the wavefront phase. Therefore, the calibration function was found in terms of the change in the wavefront, or phase change, given by

$$\Delta\phi = \frac{2\pi(\Delta n)(d)}{\lambda}, \tag{1}$$

where Δn is the RI change, λ is the wavelength of incident light, and d is the length of the modified region parallel to the optical axis. Equation (1) gives the phase change in radians, with 2π being equal to one wave of phase change at a given wavelength.[10,28] Note, $\Delta\phi\lambda$ is the 2π times the optical path difference.

IRIS structures were created in ophthalmic hydrogel material, specifically Contamac 58 (Contaflex GM Advance 58, Contamac Ltd.)*. Two types of structures were created: (1) square structures with constant phase and (2) GRIN Fresnel lenses. The first IRIS structure was a 4.5 mm square with a constant phase change (Fig. 2A). Using the calibration functions mentioned previously, IRIS parameters were chosen to induce -2π radians, or -1 wave at 535 nm, of bulk phase change in the sample. This magnitude of phase change was chosen to be consistent with the maximum phase change used in the second IRIS structure, a -2.5 D (D = 1/m = diopter) spherical Fresnel lens (Fig. 2B, 2C). IRIS was used to create continually varying phase change according to the Fresnel zone plate design shown in Fig. 2. The magnitude of phase change was found to be negative in Contamac 58 hydrogel material; thus the maximum induced phase change at the edge of each Fresnel zone, and across the central zone, was -2π radians, or -1 wave at 535 nm.

The objective used in this study had a field of view (FOV) of 1 mm. This limited FOV necessitated the use of stitching techniques to create large area refractive structures. While the scan direction was limited by the FOV, the orthogonal direction's movement was controlled by a linear stage with a range greater than 20 mm. Therefore, stitching was only necessary in the direction perpendicular to the scan direction, see Fig. 2. For the Contamac 58 samples with constant phase change (Fig. 2A), the stitching zones were set to 0.9 mm; whereas the larger Fresnel zone plates had stitching zones of 1 mm (Fig. 2B).

---

*Certain commercial equipment, instruments, or materials are identified in this paper in order to specify the experimental procedure adequately. Such identification is not intended to imply recommendation or endorsement by any of the authors' listed institutions, nor is it intended to imply that the materials or equipment identified are necessarily the best available for the purpose.

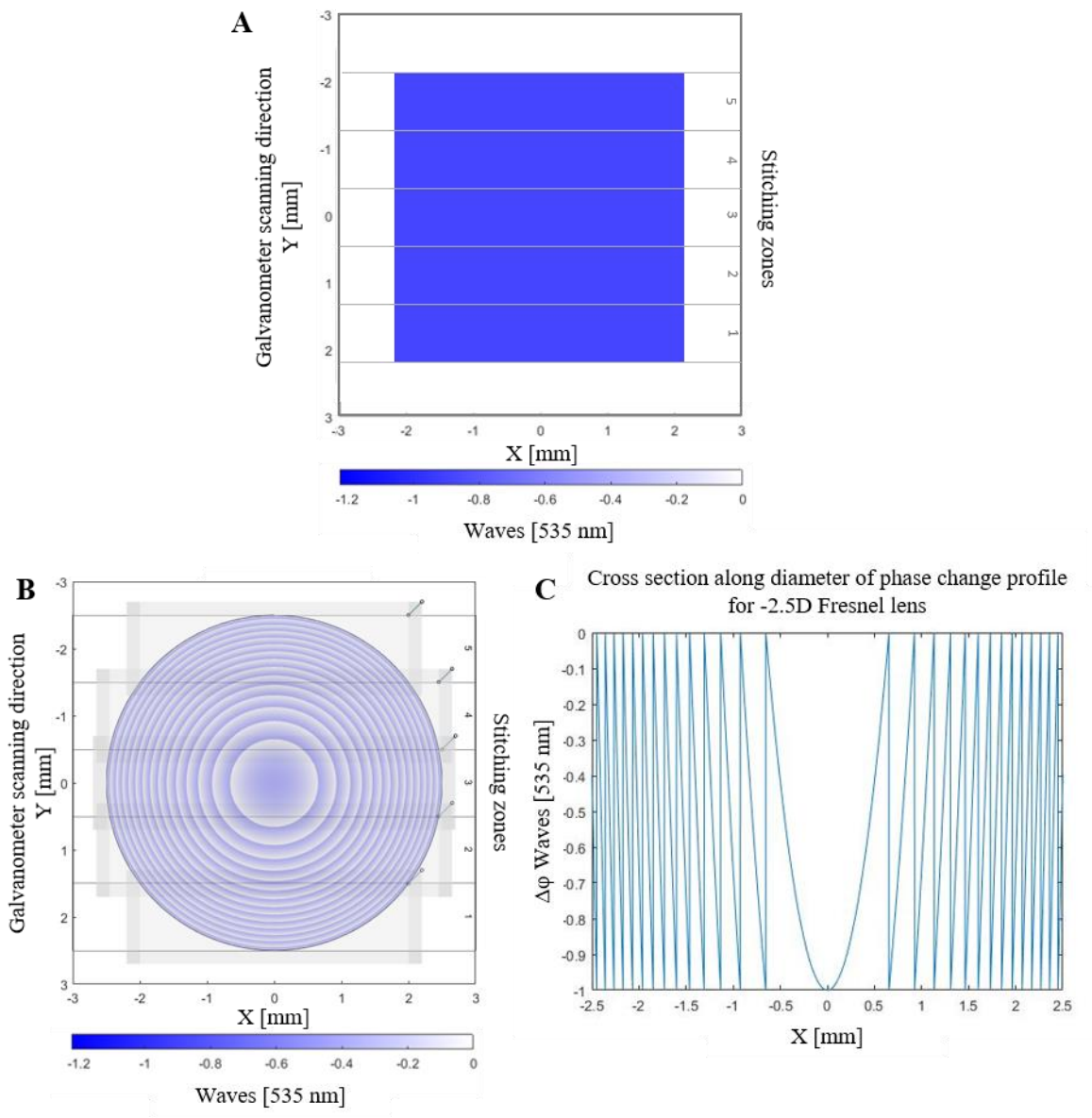

Figure 2. Two types of IRIS structures inscribed in hydrogels. A. Phase map of a 4.5 mm square with constant phase change of -2π radians, or -1 wave at 535 nm. Stitching zones were 0.9 mm. **B**. Phase map of a -2.5 D sphere, 5 mm diameter, Fresnel lens. Due to limited FOV of the microscope objective used in the IRIS procedure, five, 1 mm stitching zones were necessary. **C**. Phase profile across the diameter (Y = 0) of the Fresnel lens in (B). Full wave wrapping (2π radians = 1 wave at 535 nm) at the edge of the Fresnel zones creates a monofocal lens.

2.3 Scatter measurements

Scattering measurements were performed using the Goniometric Optical Scatter Instrument (GOSI) at the National Institute of Standards and Technology (NIST).[29] A horizontally-polarized 532 nm continuous wave laser beam passed through the sample at normal incidence and through the center of the goniometer and was slowly focused (approximately f/100) at the detector circle in the absence of the sample. A 200 µm wide, 3 mm tall slit circled the sample at a distance of 588 mm from the sample, providing the instrument with a 0.02° angular resolution along a diffraction line. Measurements were performed over a wide angle (±10° or ±20°) in the horizontal direction with step sizes of 0.01°. The data are reported normalized to the peak in the normal transmission direction, rather than by incident power and projected solid angle or projected plane angle. The hydrogel samples were sandwiched between two 1 mm thick fused silica windows

with an aqueous solution and small spacers to keep the hydrogels aligned, hydrated, but not compressed. Samples were carefully aligned by rotating them in the sample mount so that measurements were in the plane of the scan direction or the stitching direction.

In order to capture the entire scattering pattern in a single image frame, measurements were also performed using a commercial digital camera and a white screen. The camera was located near the sample and viewed the screen at an angle, resulting in some keystone distortion. The diffraction pattern from a 2D transmissive grating with approximately 1.88 µm pitch was used to correct for much of the distortion and to establish an approximate angle scale. These images were generally saturated in the peaks and the angle scale was only approximate.

3. RESULTS

Optical performance of IRIS structures was assessed first using differential interference contrast (DIC) microscopy to characterize the uniformity of RI change across IRIS patterns and to examine the integrity of the structures. Optical light scatter was then collected on the GOSI. Images of the diffraction patterns resulting from IRIS refractive structures were qualitatively compared to determine optimal IRIS parameters to reduce scatter. Finally, we asked to what degree mechanical vibrations in the IRIS instrumentation correlated with scatter in the IRIS pattern, since inconsistencies in the IRIS raster pattern could create spurious scatter effects and degrade optical quality.

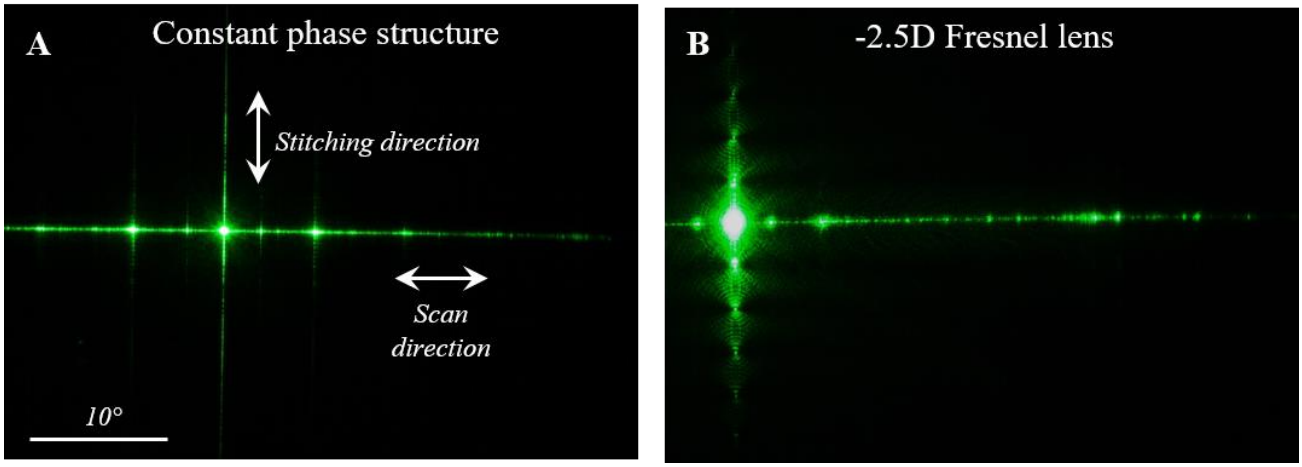

Figure 3. 2D scatter images of IRIS structures in Contamac 58 hydrogel material. A. Constant phase structure (Fig. 2A). **B.** -2.5 D sphere, Fresnel lens (Fig. 2B, 2C). IRIS parameters: 200 mm/s scan speed, 0.5 µm scan speed, -2π radian maximum phase change, or -1 wave at 535 nm, and NA = 0.19. Scale and scanning/stitching direction (double-headed arrows) are identical for both images.

We observed several scattering features in both constant phase IRIS structures (Fig. 3A), as well as GRIN Fresnel lenses (Fig. 3B). First, there was a strong line of scatter in the horizontal, scanning direction (Fig. 3) in both IRIS structures. This diffraction was most likely diffraction from the written lines and some inconsistencies along or between individual lines. These inconsistencies may be linked to certain writing parameters, including line spacing and NA, and mechanical vibrations inherent to the non-random path raster scan. At approximately 32°, outside of angular limits shown in Fig. 3A, there was a diffraction spot corresponding to a period (L = 1.0 µm) which is double the 0.5 µm line spacing parameter used to create the IRIS structures. This suggested that the galvanometer motion in one direction was not precisely the same as the motion in the reverse direction. Other distinct peaks along the horizontal streak suggested that there were specific oscillations with periods ranging from 1 µm to 30 µm. The corresponding angular location of the peaks can be found using the relationship between periodicity and angle scatter, given by

$$m\lambda = L\sin\theta_m \tag{2}$$

where m is the diffraction order, λ is the wavelength of incident light, L is the period, and the m^{th} order diffracted light will have a maxima at angle θ_m. When scatter is weak, only the first order ($m = \pm 1$) will be significant. The 2D scatter images in Fig. 3 showed diffraction peaks ranging from 1° to 32° corresponding to periods of 30 µm to 1 µm, when the incident light was 532 nm. In terms of the speed at which the lines were written when the scan spacing is 0.5 µm, 71.4 µm/s, these

periods corresponded to variations of 71 Hz to 2 Hz, respectively. It was suspected that mechanical vibrations contributed to these diffraction peaks.

We also observed lines of scatter (vertical streaks in Fig. 3) which may be the result of stitching errors (misalignment of adjacent stitched zones seen in Fig. 2) and discontinuities along Fresnel zone edges (Fig. 3B only). These vertical lines of scatter weakly replicated themselves along bright spots in the horizontal lines. The envelope of this scatter was likely related to the diffraction pattern associated with a single overlap/underlap distance at adjacent stitched zones. The manner of Fresnel zone discontinuities, either phase discontinuities or discretization of spherical zones, also affected scatter along both directions. However, scatter from these discontinuities overlapped and interfered with scatter from stitching errors, and being aperiodic, their scattering behavior was further complicated.

3.1 Scattering properties associated with line spacing and NA

To determine root causes of scatter in IRIS patterns, simple, constant phase, square structures were inscribed in hydrogels, as described in Sect. 2.2 and Fig. 2A. The total phase change across each 4.5 mm pattern was -2π radians, or 1 wave at 535 nm*. The line spacing was varied in order to determine whether line spacing inconsistencies due to mechanical vibrations in the instrumentation could result in diffractive structures within the IRIS pattern (Fig. 4).

The width of the focal spot at NA = 0.19 was about 1.3 μm. Line spacing values were chosen such that a high "fill factor" would be achieved in IRIS writing, and thus, that adjacent scan lines overlapped to create a continuous RI change across the IRIS pattern. For this reason, 0.5 μm and 0.7 μm line spacing values were investigated. Figure 4 shows the different angular distribution of diffracted light from IRIS patterns with different line spacing values.

The magnitude of scatter in both samples is not significantly different at near specular angles (<6°). However, the sample with 0.7 μm line spacing appeared to have slightly higher background scatter. The larger line spacing resulting a lower fill factor may increase background scatter, and the angular extent of scatter (Fig. 4).

While scatter extended to angles greater than 30° in both samples, the signal attenuated considerably at larger angles, which are outside the limits of Fig. 4A. Therefore, scans with the GOSI were limited to ±20°. Furthermore, dehydration of the hydrogel samples will cause deformation and thus degrade optical performance. By limiting the angular extent of the scans, the duration of the measurement was also limited, which eliminated possible spurious effects from sample dehydration.

As of this study, qualitative comparison of scatter distribution for IRIS patterns with different line spacing values showed little difference in magnitude or angular extent of diffraction. In both cases, scatter extended to approximately 28° (Fig. 4A). The magnitude of diffraction peaks in the near specular region are the same order of magnitude, with the notable exception that the 0.7 μm line spacing sample scattered strongly at about 7°, over an order of magnitude more than any nearby peaks in the 0.5 μm sample. It is worth noting that in Fig. 4B, several peaks are coincident in both diffraction patterns. All coincident peaks have nearly the same magnitude of scatter, implying that the cause of the scatter at these peaks was nominally the same for both samples, and independent of the line spacing parameter. In addition, the location of the strong diffraction peaks near the specular beam are related by the 0.5/0.7 line spacing ratio. These peaks are located at 1° and 2.6° for the 0.5 μm line spacing sample and at 0.7° and 1.8° for the 0.7 μm sample. This result supported our hypothesis that the line spacing parameter more greatly affected the angular distribution of scatter, rather than the magnitude. The coincident peaks observed may instead have been due to mechanical vibrations of the instrumentation, which are explored in a later section.

---

* It should be noted that the IRIS pattern design wavelength, 535 nm, differed slightly from the laser wavelength in the GOSI, 532 nm. This difference had minimal impact for the purposes of this study as the appropriately scaled phase change at 532 nm is 0.99 waves.

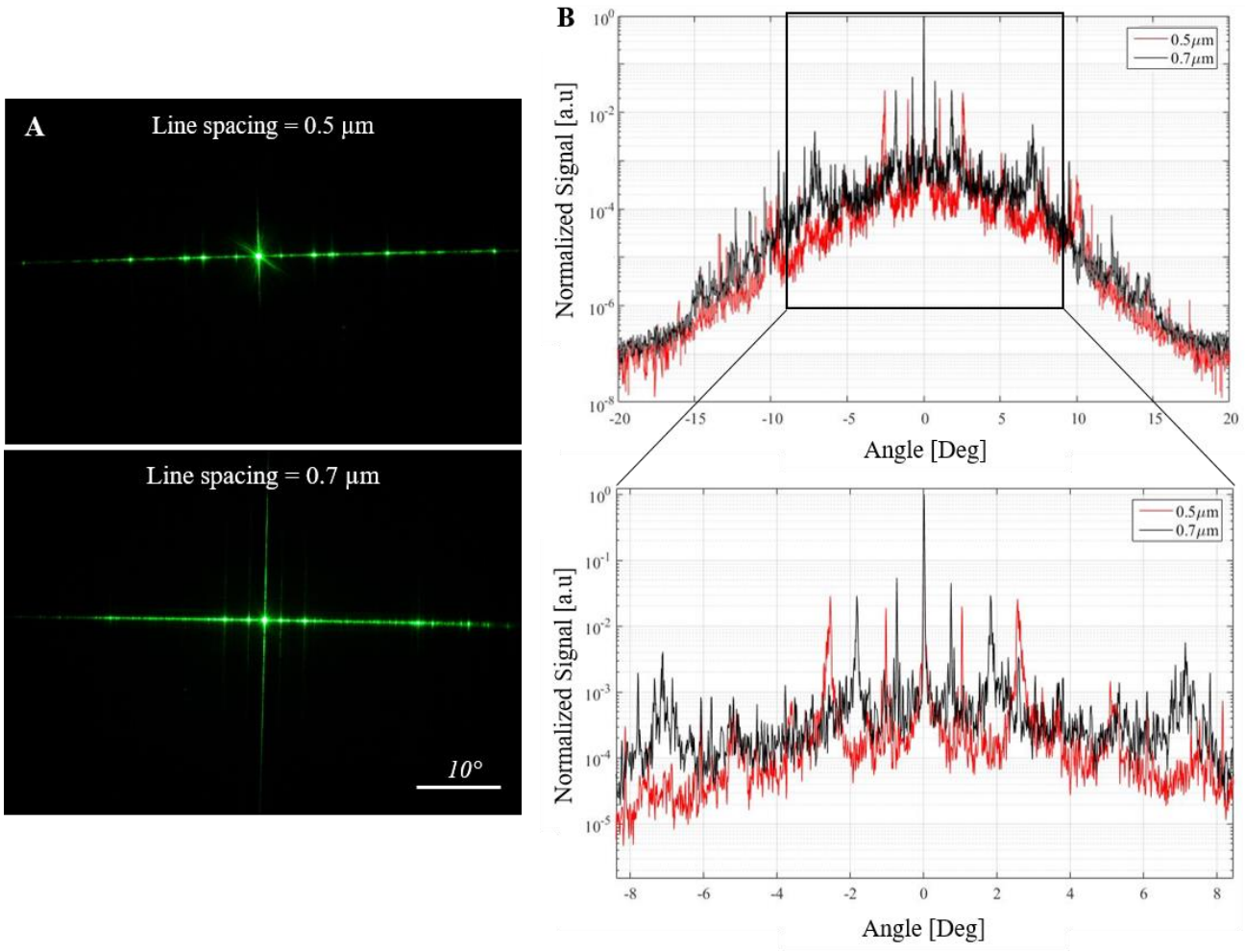

Figure 4. Diffraction patterns from flat phase structures inscribed using IRIS with different line spacing in Contamac 58 hydrogel material. A. Diffraction patterns imaged at about 550 mm from the sample using 532 nm incident light. Both samples scatter up to 28° from the specular beam. **B.** GOSI scatter measurements collected using 200 µm slit aperture, 532 nm incident light, and 0.01° increments.

One final qualitative study was performed presently using DIC microscopy to investigate the effects NA on optical quality of refractive structures (Fig. 5). Two different NA were chosen for this study, 0.19 and 0.49. A higher NA created a tighter focal spot (about 0.5 µm spot size) which directly affected the fill factor and thus caused more local modulation of the RI. Two IRIS Fresnel lenses were inscribed in Contamac 58 hydrogel material using the same parameters, except for NA = 0.19 in the first structure, and NA = 0.49 in the second. Scatter patterns were imaged in the far field with 532 nm incident light (Fig. 5A and 5D).

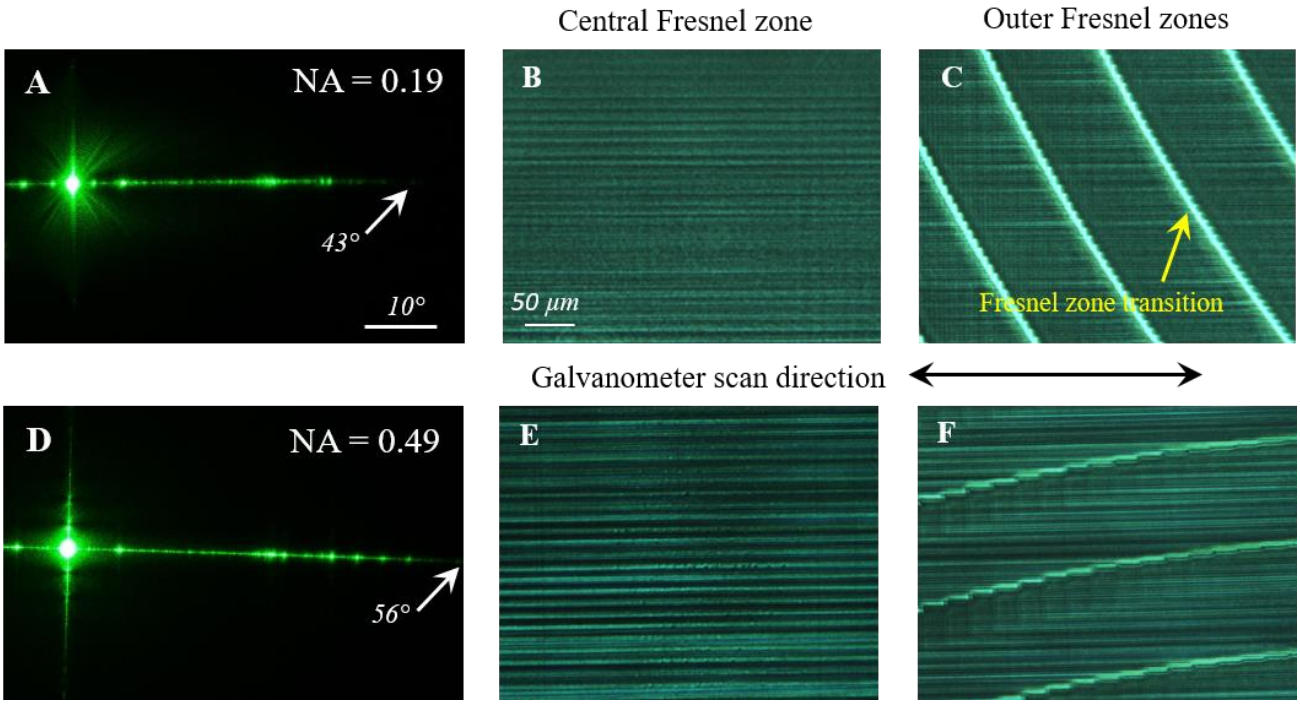

Figure 5. Visualization of optical quality of -2.5 D spherical IRIS Fresnel lenses in Contamac 58. The IRIS parameters for these lenses were: scan speed of 200 mm/s and line spacing of 0.5 µm; NA was varied between samples. **A and D.** Far field diffraction patterns from IRIS Fresnel lenses written using different NAs. Images taken about 550 mm from the sample with 532 nm incident light. **B-C and E-F.** DIC micrographs of IRIS lenticular structures. Brighter, curved lines (denoted with an arrow in **C**) represent transitions between Fresnel zones. Micrographs **B** and **E** were taken in the central Fresnel zone (area of highest phase change). Micrographs **C** and **F** were taken across outer Fresnel zones. **A-C.** NA=0.19 **D-F.** NA=0.49. Scale is the same for **A** and **D** and for all DIC micrographs.

It was evident that the optical quality of IRIS lenticular structures degraded when a higher NA was used. Comparing the two far field diffraction patterns of the lenses revealed that the higher NA IRIS lens scattered to higher angles. Specifically, the NA = 0.49 lens scattered to over 56°, whereas the lower NA IRIS lens' scatter only extended to about 43°. Furthermore, the diffraction peaks were brighter at higher angles in the high NA lens, indicating that the magnitude of scatter was also greater. Examining the lenses with DIC microscopy confirmed this result (Fig. 5). Under a DIC microscope, a structure with a continuous phase change profile would appear uniformly bright. Variations in brightness across an IRIS structure indicated variations in induced phase change. While both sets of DIC micrographs showed some variation in brightness across the IRIS structures, the distinct periodic structure of bright and dark lines in Fig. 5E and 5F illustrated the discontinuous nature of the induced phase change in the IRIS pattern written at NA = 0.49. Moreover, the spot size was approximately equal to the line spacing for the NA = 0.49 sample. Any long-period variations along the scan direction will affect the fill factor more than in the NA = 0.19 case, where the spot size is more than double the line spacing. The phase change in the low NA lens (Fig. 5B, 5C) was more continuous because of this. Thus, our results shown above indicated that RI change integrity may be vital in controlling the optical quality of IRIS lenses, since this phase change irregularity could be seen to manifest as increased diffraction in Fig. 5D. These results further implied that NA was one of the most important IRIS parameters in terms of reducing light scatter. By lowering the NA, the fill factor was increased, thus creating a more continuous refractive structure, which seems to reduce the extent and magnitude of scatter.

3.2 Scattering from stitching errors

As mentioned previously, the limited FOV of the microscope objective used in the IRIS procedure necessitated stitching in a direction orthogonal to the galvanometer scanning to create large area refractive structures. Registration errors in the linear stages may produce stitching errors, wherein adjacent stitched sections may overlap slightly, or leave a small gap between stitched sections. Examples of both these stitching errors were observed under DIC microscopy (Fig. 6A), with error magnitudes ranging from 5 µm to 20 µm. Here, we tested the hypothesis that these small registration errors may create spurious diffraction in a direction orthogonal to diffraction from the scan lines. The observed diffraction pattern

(Fig. 6C) confirmed that this was indeed the case, as did scatter data collected from the stitching direction as compared to diffraction from the scan direction, measured by the GOSI (Fig. 6B).

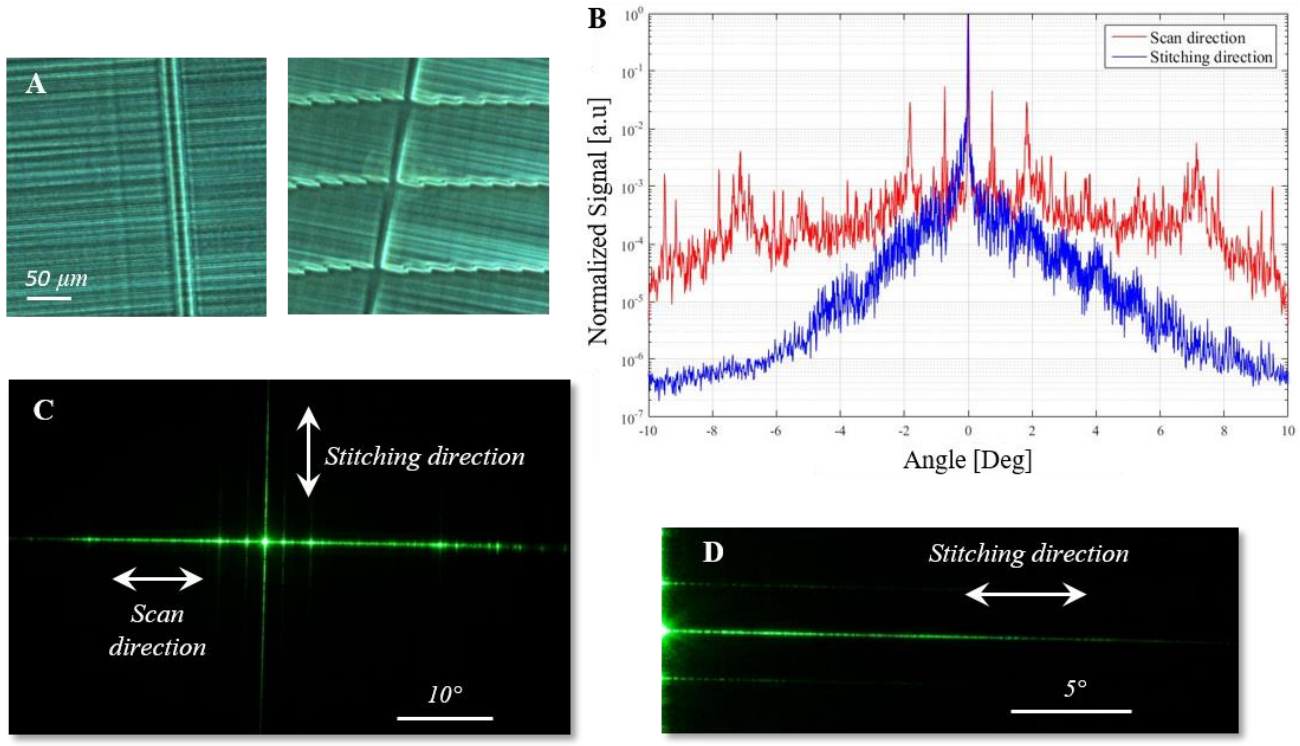

Figure 6. Observations of stitching errors. **A.** DIC microscope images of two stitching errors, resulting in either stitched zone overlap (left) or a gap between adjacent zones (right). **B.** GOSI scatter measurements of diffraction from the scan direction (red) or stitching direction (blue) collected using 200 μm slit aperture, 532 nm incident light, at 0.01° increments. **C.** 2D diffraction pattern of constant phase IRIS structure with 0.9 mm stitched zones. Incident laser light is 532 nm; imaged at about 550 mm from the sample. **D.** Diffraction from the stitching direction displayed a periodic structure.

Scatter was clearly evident orthogonal to the scatter induced by the scan lines as a vertical streak (Fig. 6C); however, no distinct diffraction peaks were discernable. There was, instead, a distinct periodic nature to the diffraction, with an envelope that may be related to the magnitude of the stitched zone misalignment (Fig. 6A, 6D). The magnitude of scatter along the stitching direction attenuated away from the specular beam to be over two orders of magnitude less than scatter seen from the scan lines. These two facts potentially indicated that stitching errors were not likely to be the dominant source of degradation of optical quality in IRIS lenticular structures. Nonetheless, improved registration between linear stages, the galvanometer, and the AOM intensity control should reduce the magnitude of stitching errors, with the goal of eliminating them completely in future iterations of the instrumentation being developed for this procedure in humans.

3.3 Effect of Fresnel zone discontinuities on scatter

Fresnel zone discontinuities represent yet another possible source of scatter in IRIS lenticular structures. The Fresnel zones have a phase discontinuity at the edge of each zone (Fig. 2C) which may act as a diffraction edge. In addition, the process of converting the analytical wavefront to a discrete point map for the IRIS exposure and stage parameters also created a discretized Fresnel zone transition. While the stages used presently had high precision and accuracy, the number of points loaded into the file used to synchronize the linear stages, the 2D galvanometer, and the AOM output (for laser intensity control) combined to create discontinuities along the edges of Fresnel zones. The motion of the focal spot was limited to 2D orthogonal motion. Therefore, to create spherical Fresnel zones, the edges of the zones became discretized, which can be seen as a "staircase" structure in DIC (Fig. 7A, 7B). The size of the discrete steps was dependent on hardware limitations, namely the number of points the digital acquisition card could hold to create the IRIS structure. A larger number of points reduced the size of the discrete steps to create circular Fresnel zones. For this study, two different discrete

step sizes were studied. In the first, the discrete steps were 25 µm (Fig. 7A, 7C). In the second, we increased the number of points used to define the IRIS structure by a factor of 5, reducing the step size to 5 µm (Fig. 7B, 7D).

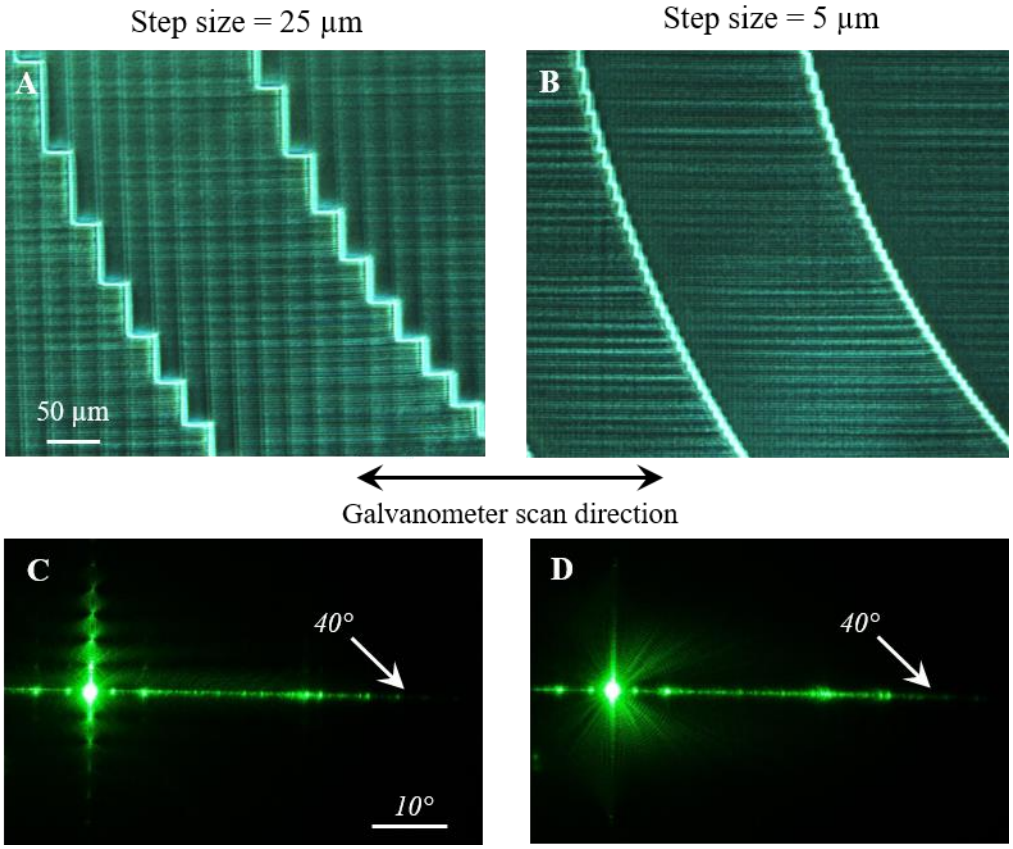

Figure 7. DIC microscope images of two IRIS lenticular structures in Contamac 58 and resulting 2D scatter patterns imaged in the far field. A. Fresnel zone edges with a larger discrete steps. Step size of 25 µm. **B.** Same Fresnel structure as **A**, but with smaller discrete steps along Fresnel zone edges. Step size of 5 µm. Scale is the same for both images. **C.** 2D scatter pattern of IRIS lens with 25 µm step size displayed increased scatter in the direction orthogonal to the diffraction from the galvanometer scan direction. **D.** 2D scatter pattern of IRIS lens with 5 µm step size displayed less scatter in the vertical streak than **C**. Both **C** and **D** images were collected about 550 mm from the sample with 532 nm incident light. Scale is the same for both images.

The 2D discretization of the spherical Fresnel zones manifested in the 2D scatter pattern of IRIS lenticular structures (Fig. 7C, 7D). The Fresnel zone transitions in the smaller step size sample (Fig. 7B) displayed a smoother boundary between zones, whereas the larger step size used to discretize the analytical wavefront created a coarser staircase structure at the boundaries (Fig. 7A). The larger step size created a highly aperiodic structure in the vertical direction, parallel to the stitching zone boundaries which were seen to influence scatter described in the previous section. In constant phase structures, the only periodic structure that could result in scatter along that direction was stitching errors. However, due to the discretization of the spherical Fresnel zones, the "staircase" structure creates periodic discontinuities along the stitching and the galvanometer scan directions. This resulted in increased scatter along both streaks. The horizontal diffraction streak from constant phase structures only scattered to approximately 28° (Fig. 4), whereas IRIS lenticular structures' scatter extended to approximately 40°. Furthermore, the larger step size enhanced the magnitude of scatter in the vertical direction significantly (Fig. 7C). To summarize, our data suggest that a smaller step size helped reduce scatter from Fresnel zone discontinuities and resulted in a less intense 2D scatter pattern. The reduction was more pronounced in the stitching direction. This supported our hypothesis that the vertical, aperiodic structure related to the larger step size negatively impacted scatter in the stitching direction.

Finally, we should note that the 2D scatter patterns were imaged by passing nearly collimated laser light through the -2.5 D IRIS lenses, at a distance of approximately 550 mm from the sample. No compensating optics were used to account for the diverging nature of the IRIS lenses. Therefore, the resulting patterns were the defocused image of the scatter patterns, which may account for the slightly larger angular extent along both diffraction streaks, and the large blurring of the specular beam.

3.4 Vibrational analysis of IRIS instrumentation

From the previous sections, it is clear that the scatter from IRIS lenticular structures can be attributed to several IRIS writing parameters, such as Fresnel zone discontinuities, line spacing irregularities, and stitching errors. One of the major inferences from our results so far, was that mechanical vibrations in the scanning system could represent a significant source of optical scatter in IRIS patterns. The raster path, like any other non-random tool path, is susceptible to mechanical oscillations. Similar to mid-spatial frequency errors found in sub-aperture grinding and polishing processes,[30] periodic motion in the system can produce undesirable optical effects in the final lens pattern.

In order to better understand the source of vibrations in our system, accelerometers were placed in various locations on the IRIS machine. Our primary goal was to assess whether the major sources of vibrations affecting the IRIS patterns were inherent to the system or stemmed from external sources. For this study, all of the lenticular and constant phase structures were created with the sample mounted on a long cantilevered arm, underneath the objective. Minimal vibration isolation was employed, as would be consistent with expected clinical implementation of IRIS in living tissue. After gathering initial scatter data, and seeing evidence of mechanical vibrations within the IRIS system, a new configuration was devised in which the sample was mounted to a shorter, stiffer, cantilevered arm and vibration isolation was improved to reflect IRIS implementation as a scalable, ophthalmic hydrogel manufacturing process. Tests were conducted with accelerometers mounted in both configurations, the original configuration and the improved, stiffer, isolated configuration. In both cases, the accelerometers were placed normal to the mounting surface. As both mounting platforms were cantilevered beams, the greatest motion was anticipated to be normal to the mounting surface. Trials were two minutes in length and collected at a 10 kHz sampling rate. The accelerometer's functional range was 0.15 Hz to 1 kHz.

The frequency response of two accelerometers under baseline conditions (*i.e.*, background vibrations, no purposeful excitation) was measured (Fig. 8A) and the amplification ratio between the two conditions was calculated (Fig. 8B). In this ratio, the case using the short platform with passive vibration isolation was in the numerator ("High Stiffness, Isolated"), while the case using the long platform with minimal vibration isolation was in the denominator ("Low Stiffness, Unisolated"). This ratio indicated the amplification (or attenuation) of the vibrations across the frequency spectrum. By comparing these two signals, we were able to visualize the anticipated reduction in undesirable vibrations at critical frequencies across the 10 Hz to 40 Hz range, with a smaller increase in the magnitude of vibrations at higher frequencies. If these vibrations translated to inconsistencies along or between the scan lines, they would also affect the optical scatter generated by the samples. To further visualize the reduction in vibrations, the cumulative amplitude spectrum (CAS) was calculated for the data shown in Fig. 8A. As the frequency increases, the CAS includes all cumulative contributions up until that frequency value (Fig. 8C). After approximately 10 Hz, the cumulative effect of the vibrations was significantly lower for the "High Stiffness, Isolated" case. Despite the amplification shown at some higher frequency values in the PSD ratio in Fig. 8B, the CAS values for "High Stiffness, Isolated" case remained well below the values for the "Low Stiffness, Unisolated" case. Therefore, the CAS supports our hypothesis that stiffer sample mounting and vibration isolation may lead to improved optical results in IRIS-treated hydrogels.

By comparing two samples written under the two different sample mounting configurations with DIC microscopy, it became clear that the optical quality and RI change integrity of the sample written with the "High Stiffness, Isolated" (Fig. 8D, bottom) sample mounting conditions was significantly better than that seen when the sample was mounted using the "Low Stiffness, Unisolated" configuration (Fig. 8D, top). The two bars of constant phase seen in Fig. 8C and 8D were written using the same IRIS parameters (200 mm/s scan speed, 0.5 μm line spacing, and 100 mW of average laser power); yet the consistency of phase change seen under DIC differed greatly depending on the sample mounting configuration. The low stiffness, minimal isolation configuration appeared less continuous, showing a periodic difference in phase change. The stiffer mounting configuration had a higher natural frequency, and the improved isolation reduced the impact of external excitations, leading to higher quality optical structures. This test confirmed the hypothesis that mechanical vibrations translate directly into inconsistencies along scan lines that reduce optical quality and may result in increased scatter. Further study of samples written under "High Stiffness, Isolated" mounting conditions must be conducted to assess possible implications in terms of optical scatter from IRIS structures.

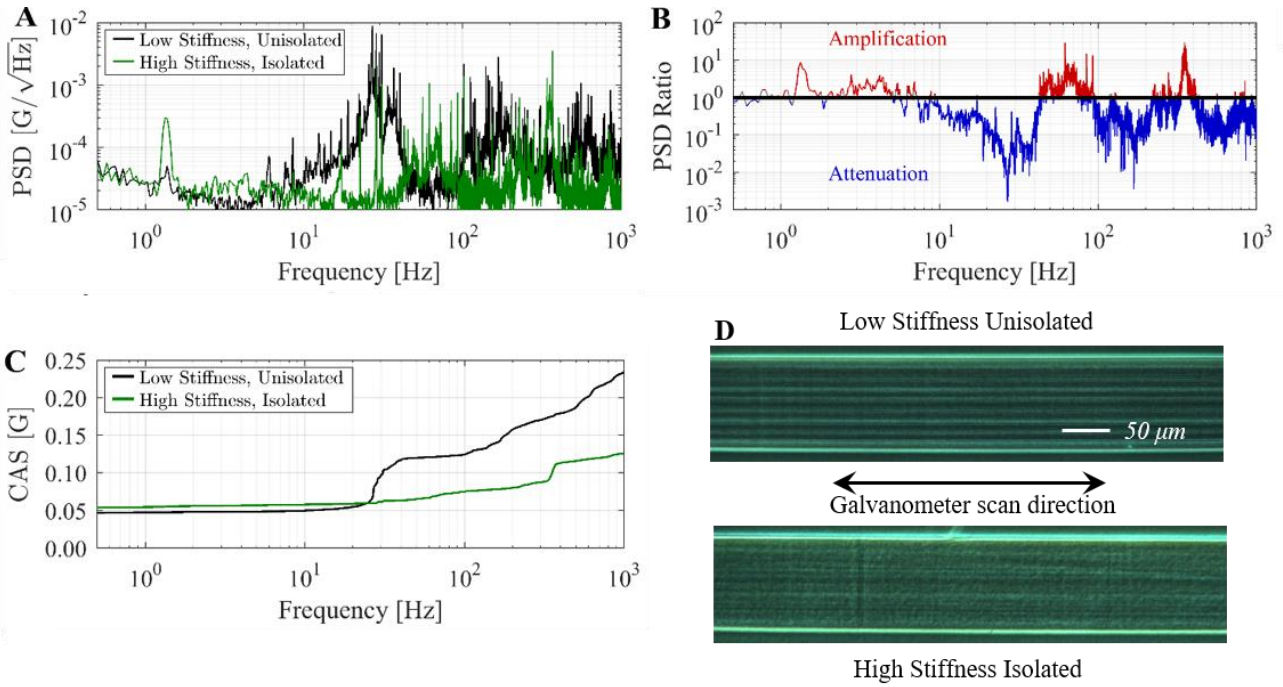

Figure 8. Improved sample mounting configuration reduced vibrations from instrumentaion and led to higher quality IRIS structures. **A.** Frequency response of the accelerometers in two conditions. In the "High Stiffness, Isolated" case, passive vibration isolation was employed and a short cantilevered beam was used to hold the sample. In the "Low Sitfness, Unisolated" case, minimal vibration isolation was employed, and a long cantilevered beam was used to hold the sample. **B.** Amplifcation ratio between the high stiffness, isolated case and the low stiffness, unisolated case as a function of frequency, plotted on a logarithmic scale. **C.** Cumulative amplitude spectrum calculated from the data in A the total overall vibrations from higher frequencies were reduced by implementing the stiffer, isolated. **D.** DIC micrograph of constant phase bar in Contamac 58 inscribed under original mounting conditions (top) showed periodic variations in phase change. DIC micrograph of constant phase bar written using the same IRIS parameters, but with improved vibration isolation and sample mounting configuration showed smooth, continous phase change (bottom). Scale is the same for **C** and **D**.

4. DISCUSSION

IRIS is a novel technique and could represent a new process for high-throughput contact lens and intraocular lens manufacturing. Furthermore, it could offer a new, non-surgical method for human vision correction when performed directly in the cornea. By altering the RI of cornea rather than ablating its anterior surface to correct for vision errors, IRIS presents fewer risks of post-operative side effects than those associated with LASIK and PRK.[19] However, if optical scatter is not addressed in IRIS applications, other negative consequences may result. The present study aimed to elucidate relevant IRIS parameters for reducing optical scatter and improving visual performance by studying IRIS lenticular structures in tissue-surrogate hydrogels.

Light can be scattered by imperfections in a contact lens, the cornea, or an intraocular lens and this scatter can result in lowered contrast sensitivity and visual acuity, as well as glare.[23-25,31,32] For example, functional vision performance can be negatively impacted due to corneal changes following LASIK.[33] Specifically, corneal backscatter can increase following flap creation in LASIK, negatively impacting the patient's vision immediately following surgery.[34] Another study was conducted, examining low-contrast acuity and light scatter in different forms of myopic correction.[22] Soft contact lenses resulted in increased light scatter and worse mean acuity than any other form of vision correction, including hard contact lenses, spectacles, and eyes following excimer laser ablation.[22] Since the IRIS procedure can be performed in both ophthalmic hydrogels and cornea, any imperfections that result in scatter may cause similar detrimental effects in terms of functional vision.

The present results identify four sources of scatter in IRIS lenticular structures inscribed into hydrogel materials: (1) line spacing and NA; (2) stitching errors, resulting from adjacent scanning fields not properly aligned to one another; (3) diffraction from Fresnel zone discontinuities, and (4) long-period variations in induced phase change, likely due to

inconsistences along the scan lines generated by the writing instrument. Imperfections created by mechanical vibrations in the IRIS instrumentation or a low fill factor were linked directly with optical scatter. Reducing these imperfections will hopefully lead to improved optical performance in ophthalmic applications.

In general, varying the line spacing parameter was found to have little effect on the optical quality of IRIS structures. However, when coupled with NA, the line spacing parameter directly affected the fill factor, which adversely affected scatter if it was too low. Therefore, a low NA was deemed optimal for improved IRIS structure performance in hydrogels. Phase change continuity across IRIS structures was also linked to scatter. NA, line spacing inconsistencies, and mechanical vibrations all seemed to contribute to optical integrity of IRIS patterns. By stiffening the sample mount, isolating the system from external excitations, and employing a low NA for a high fill factor, IRIS structures can be optimized to reduce scatter and improve optical integrity. Future studies are underway to explore implementation of such improvements in hydrogel materials, and their translation to cornea.

The focal spot of the laser, along with the line spacing parameter may also be key parameters for reducing higher angle scatter in IRIS structures. Since the focal spot of the laser is raster scanned through the sample, minor differences in the positive and negative galvanometer motion may translate to variations in adjacent lines that have the potential to create diffraction gratings with a pitch equal to twice the line spacing. While a 0.5 μm pitch grating will not diffract at 532 nm, a 1 μm pitch grating will have first order diffraction at 32.3°. A grating with a period of 0.7 μm will have first order diffraction at 49.5°, but a 1.4 μm (twice 0.7 μm) grating will diffract at 22.3°. By using a tighter line spacing, it may be possible to eliminate diffraction from the native line spacing pitch at the center of the visual wavelength range; however, more work must be performed to investigate larger angle scatter and what effect line spacing may have in creating or mitigating higher angle scatter.

For IRIS Fresnel lenses, the manner in which the analytical wavefront transformed into a discrete point map affected the overall scatter of the sample, along both the scanning and stitching directions. A larger step size created aperiodic structures in both directions, which amplified scatter along the two diffraction streaks. By reducing the step size to 5 μm, the discontinuities along the Fresnel zones were also decreased, which improved the optical performance of IRIS lenses by minimizing scatter along the stitching direction. In future IRIS instrumentation, specifically for human vision correction, improved hardware should reduce or eliminate registration errors between motion stages and intensity control to reduce or eliminate scatter due to stitching errors. This, in combination with a small step size when creating the discrete point map for IRIS lenses will positively affect visual performance through IRIS structures in both hydrogel and corneal tissue.

The present results also showed that mechanical vibrations were responsible for several of the diffraction peaks seen in IRIS structures. Particularly, coincident peaks from samples written with different line spacing values support this notion. Closer examination of diffraction patterns from flat phase structures showed similar scatter trends in samples with different line spacings. In Fig. 4B, the near angular scatter patterns appear to be scaled versions of one another, with the angular distribution of the 0.7 μm line spacing sample being slightly more spread out than the 0.5 μm sample. Since the speed of the linear stages used to create the line spacing was different for the two samples (71.4 mm/s for 0.5 μm line spacing and 100 mm/s for 0.7 μm line spacing) the frequency of the mechanical vibrations may be shifted, which would result in slightly different angular distribution of scatter. Further work has begun that aims to separate scatter effects due to instrumentation and scatter produced by IRIS refractive patterns.

The improvement in phase change continuity seen in DIC with the improved sample mounting configuration can be linked to the frequency response of the system. From the accelerometer data, it was clear that the major resonance of the original sample mounting configuration was in the 10 Hz to 40 Hz range, and that improved sample mounting attenuated that frequency range considerably (Fig. 8A, B). If those excited resonances in that range were directly translated into the IRIS pattern, the frequency response of the system in that range would generate diffraction peaks between 4° and 17°. We hypothesized that mechanical vibrations would cause coincident diffraction peaks between samples with different IRIS parameters. The scatter data collected from the flat phase structures in Section 3.1 showed coincident, distinct, broad diffraction peaks in that range, supporting our hypothesis. Studies are now underway to ascertain the link between instrumentation frequency response and its translation to optical scatter.

The present results have important implications for optimizing writing parameters and instrumentation in an effort to reduce light scatter from IRIS lenticular structures. They provide clear direction by highlighting the fact that a key requirement for improving optical quality may be to increase phase change continuity across IRIS patterns. The negative impact of scatter in ophthalmic applications is clear, although future studies should focus on directly measuring the

scattering properties of IRIS structures together with their effects on visual acuity and contrast sensitivity. Ultimately, by understanding what drives scattering effects in IRIS, future applications in both ophthalmic hydrogels and cornea will be improved.

5. CONCLUSIONS

This study examined several possible sources of light scatter resulting from IRIS lenticular structures in ophthalmic hydrogels. Understanding the sources of scatter and mitigating them is an important step toward making IRIS a scalable manufacturing technique for ophthalmic applications, including contact lenses, intraocular lenses, and ultimately, for optimizing corneal vision correction.

The present study focused on the scattering properties of hydrogels as tissue surrogates. Our results elucidate key IRIS parameters that induce optical scatter, providing us with specific recommendations that should lead to improved IRIS lenticular structures. Specifically, we now know that lowering the NA will reduce the magnitude and angular extent of diffraction. A low NA coupled with a line spacing of 0.5 μm will create a high fill factor, resulting in a continuous RI change and thus reducing diffraction as well. Hardware improvements that allow for more continuous Fresnel zone edges will reduce diffraction in the orthogonal direction from scan line diffraction. Finally, long-period vibrations arising from mechanical resonances in the IRIS instrumentation should be mitigated through improved vibration isolation and by increasing sample holder stiffness. As an immediate next step, the next phase of our research will implement these modifications and determine their effects on reducing scatter from IRIS lenses in both hydrogels and living cornea.

ACKNOWLEDGEMENTS

This project was supported by an unrestricted grant to the University of Rochester's Department of Ophthalmology from the Research to Prevent Blindness (RPB) Foundation, by the National Institutes of Health (R01 grant EY015836 to KRH; Core grant P30 EY01319F to the Center for Visual Science); by the National Science Foundation (grants IIP:1549700 and IIP:1738506), by a grant from Clerio Vision, Inc. with matching funds from the University of Rochester's Center for Emerging & Innovative Sciences, a NYSTAR-designated Center for Advanced Technology, and by an Incubator Grant from the University of Rochester's CTSI Scientific Advisory Committee (SAC).

The authors declare the following interests: K.R. Huxlin, and J. D. Ellis have founder's equity in Clerio Vision, Inc., which partially supported this research. S.C. Butler has equity in Clerio Vision, Inc. K. R. Huxlin and J. D. Ellis have no fiduciary responsibility in Clerio Vision, Inc.

REFERENCES

[1] R. R. Gattass, and E. Mazur, "Femtosecond laser micromachining in transparent materials," Nature photonics, 2(4), 219-225 (2008).

[2] K. Yamada, W. Watanabe, T. Toma *et al.*, "In situ observation of photoinduced refractive-index changes in filaments formed in glasses by femtosecond laser pulses," Optics letters, 26(1), 19-21 (2001).

[3] A. Baum, P. J. Scully, M. Basanta *et al.*, "Photochemistry of refractive index structures in poly (methyl methacrylate) by femtosecond laser irradiation," Optics letters, 32(2), 190-192 (2007).

[4] K. M. Davis, K. Miura, N. Sugimoto *et al.*, "Writing waveguides in glass with a femtosecond laser," Optics Letters, 21(21), 1729-1731 (1996).

[5] G. Cerullo, R. Osellame, S. Taccheo *et al.*, "Femtosecond micromachining of symmetric waveguides at 1.5 μm by astigmatic beam focusing," Optics Letters, 27(21), 1938-1940 (2002).

[6] C. B. Schaffer, A. Brodeur, J. F. García *et al.*, "Micromachining bulk glass by use of femtosecond laser pulses with nanojoule energy," Optics letters, 26(2), 93-95 (2001).

[7] C. B. Schaffer, J. F. García, and E. Mazur, "Bulk heating of transparent materials using a high-repetition-rate femtosecond laser," Applied Physics A, 76(3), 351-354 (2003).

[8] K. Minoshima, A. M. Kowalevicz, E. P. Ippen *et al.*, "Fabrication of coupled mode photonic devices in glass by nonlinear femtosecond laser materials processing," Optics Express, 10(15), 645-652 (2002).

[9] L. Ding, R. Blackwell, J. F. Kunzler *et al.*, "Large refractive index change in silicone-based and non-silicone-based hydrogel polymers induced by femtosecond laser micro-machining," Optics express, 14(24), 11901-11909 (2006).

[10] G. A. Gandara-Montano, A. Ivansky, D. E. Savage *et al.*, "Femtosecond laser writing of freeform gradient index microlenses in hydrogel-based contact lenses," Optical Materials Express, 5(10), 2257-2271 (2015).

[11] L. G.-M. Zheleznyak, Gustavo; MacRae, Scott; Huxlin, Krystel R.; Ellis, Jonathan D.; Geunyoung, Yoon; Knox, Wayne H., "First demonstration of human visual performance through refractive-index-modified ophthalmic devices written in hydrogels."
[12] J. D. Ellis, D. R. Brooks, K. Wozniak *et al.*, "Manufacturing of Gradient Index Lenses for Ophthalmic Applications," OSA Technical Digest (online). OW1B.3.
[13] L. Ding, W. H. Knox, J. Bühren *et al.*, "Intratissue refractive index shaping (IRIS) of the cornea and lens using a low-pulse-energy femtosecond laser oscillator," Investigative ophthalmology & visual science, 49(12), 5332-5339 (2008).
[14] K. T. Wozniak, S. M. Gearhart, D. E. Savage *et al.*, "Comparable change in stromal refractive index of cat and human corneas following blue-IRIS," Journal of Biomedical Optics, 22(5), 055007-055007 (2017).
[15] L. Xu, W. H. Knox, and K. R. Huxlin, "Exogenous and endogenous two-photon absorption for Intra-tissue Refractive Index Shaping (IRIS) in live corneal tissue [Invited]," Optical Materials Express, 1(7), 1159-1164 (2011).
[16] D. E. Savage, D. R. Brooks, M. DeMagistris *et al.*, "First demonstration of ocular refractive change using blue-iris in live cats," Investigative ophthalmology & visual science, 55(7), 4603 (2014).
[17] L. Xu, W. H. Knox, M. DeMagistris *et al.*, "Noninvasive intratissue refractive index shaping (IRIS) of the cornea with blue femtosecond laser light," Investigative ophthalmology & visual science, 52(11), 8148 (2011).
[18] L. J. Nagy, L. Ding, L. Xu *et al.*, "Potentiation of femtosecond laser intratissue refractive index shaping (IRIS) in the living cornea with sodium fluorescein," Investigative ophthalmology & visual science, 51(2), 850 (2010).
[19] K. T. Wozniak, N. Elkins, D. R. Brooks *et al.*, "Contrasting cellular damage after Blue-IRIS and Femto-LASIK in cat cornea," Experimental Eye Research, 165, 20-28 (2017).
[20] L. Ding, L. J. Nagy, L. Xu *et al.*, "Enhancement of intra-tissue refractive index shaping (IRIS) of the cornea by two-photon absorption." CWE4.
[21] L. Xu, K. R. Huxlin, M. DeMagistris *et al.*, "Non-invasive Blue Intra-tissue Refractive Index Shaping (IRIS) in Living, Excised Cornea." PDPA11.
[22] C. P. Lohmann, F. Fitzke, D. O'Brart *et al.*, "Corneal light scattering and visual performance in myopic individuals with spectacles, contact lenses, or excimer laser photorefractive keratectomy," American journal of ophthalmology, 115(4), 444-453 (1993).
[23] K. Miyata, M. Honbo, S. Otani *et al.*, "Effect on visual acuity of increased surface light scattering in intraocular lenses," Journal of Cataract & Refractive Surgery, 38(2), 221-226 (2012).
[24] D. Miller, E. Wolf, S. Geer *et al.*, "Glare sensitivity related to use of contact lenses," Archives of Ophthalmology, 78(4), 448-450 (1967).
[25] D. B. Elliott, S. Mitchell, and D. Whitaker, "Factors affecting light scatter in contact lens wearers," Optometry & Vision Science, 68(8), 629-633 (1991).
[26] D. R. Brooks, N. S. Brown, D. E. Savage *et al.*, "Precision large field scanning system for high numerical aperture lenses and application to femtosecond micromachining of ophthalmic materials," Review of Scientific Instruments, 85(6), 065107 (2014).
[27] K. T. Wozniak, S. M. Gearhart, D. E. Savage *et al.*, [Comparable Change in Stromal Refractive Index of Cat and Human Corneas Following Blue-IRIS], Journal of Biomedical Optics(2017).
[28] G. A. Gandara-Montano, V. Stoy, M. Dudič *et al.*, "Large optical phase shifts in hydrogels written with femtosecond laser pulses: elucidating the role of localized water concentration changes," Optical Materials Express, 7(9), 3162-3180 (2017).
[29] T. A. Germer, and C. C. Asmail, "Goniometric optical scatter instrument for out-of-plane ellipsometry measurements," Review of scientific Instruments, 70(9), 3688-3695 (1999).
[30] D. Aikens, J. E. DeGroote, and R. N. Youngworth, "Specification and control of mid-spatial frequency wavefront errors in optical systems." OTuA1.
[31] G. T. Timberlake, M. G. Doane, and J. H. Bertera, "Short-term, low-contrast visual acuity reduction associated with in vivo contact lens drying," Optometry & Vision Science, 69(10), 755-760 (1992).
[32] S. V. Patel, K. H. Baratz, D. O. Hodge *et al.*, "The effect of corneal light scatter on vision after Descemet stripping with endothelial keratoplasty," Archives of ophthalmology (Chicago, Ill.: 1960), 127(2), 153-160 (2009).
[33] J. T. Holladay, D. R. Dudeja, and J. Chang, "Functional vision and corneal changes after laser in situ keratomileusis determined by contrast sensitivity, glare testing, and corneal topography," Journal of Cataract & Refractive Surgery, 25(5), 663-669 (1999).

[34] S. V. Patel, L. J. Maguire, J. W. McLaren *et al.*, "Femtosecond laser versus mechanical microkeratome for LASIK: a randomized controlled study," Ophthalmology, 114(8), 1482-1490 (2007).